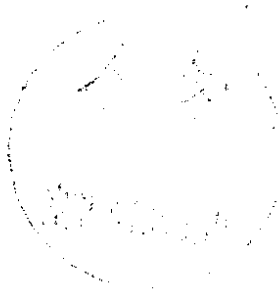


**COMPARISON OF FORWARD HADRONS PRODUCED IN MUON INTERACTIONS ON NUCLEAR TARGETS AND DEUTERIUM***The European Muon Collaboration*Aachen<sup>1</sup>, CERN<sup>2</sup>, Freiburg<sup>3</sup>, MPI Heidelberg<sup>4</sup>, Lancaster<sup>5</sup>, LAPP (Annecy)<sup>6</sup>, Liverpool<sup>7</sup>, Marseille<sup>8</sup>, Mons<sup>9</sup>, Oxford<sup>10</sup>, RAL (Chilton)<sup>11</sup>, Sheffield<sup>12</sup>, Torino<sup>13</sup>, Uppsala<sup>14</sup>, Warsaw<sup>15</sup>, Wuppertal<sup>16</sup>, Yale<sup>17</sup>

J. Ashman<sup>12</sup>, B. Badelek<sup>15a</sup>, G. Baum<sup>17b</sup>), J. Beaufays<sup>2c</sup>), C.P. Bee<sup>7</sup>, C. Benchouk<sup>8</sup>, I.G. Bird<sup>4d</sup>), S.C. Brown<sup>7e</sup>), M.C. Caputo<sup>17f</sup>), H.W.K. Cheung<sup>10g</sup>), J.S. Chima<sup>11h</sup>), J. Ciborowski<sup>15a</sup>), R. Clift<sup>11</sup>, G. Coignet<sup>6</sup>, F. Combley<sup>12</sup>, G. Court<sup>7</sup>, G. d'Agostini<sup>8</sup>, J. Drees<sup>16</sup>, M. Düren<sup>4</sup>, N. Dyce<sup>5</sup>, A.W. Edwards<sup>16i</sup>), M. Edwards<sup>11</sup>, T. Ernst<sup>3</sup>, M.I. Ferrero<sup>13</sup>, D. Francis<sup>7</sup>, E. Gabathuler<sup>7</sup>, R. Gamet<sup>7</sup>, V. Gibson<sup>10j</sup>), J. Gillies<sup>10k</sup>), P. Grafström<sup>14j</sup>), K. Hamacher<sup>16</sup>, D. von Harrach<sup>4l</sup>), P. Hayman<sup>7</sup>, J.R. Holt<sup>7</sup>, V.W. Hughes<sup>17</sup>, A. Jacholkowska<sup>2m</sup>), T. Jones<sup>7k</sup>), E.M. Kabuss<sup>4l</sup>), B. Korzen<sup>16</sup>, U. Krüner<sup>16</sup>, S. Kullander<sup>14</sup>, U. Landgraf<sup>3</sup>, D. Lanske<sup>1</sup>, F. Lettenström<sup>14n</sup>), T. Lindqvist<sup>14</sup>, J. Loken<sup>10</sup>, M. Matthews<sup>7</sup>, Y. Mizuno<sup>4o</sup>), K. Mönig<sup>16</sup>, F. Montanet<sup>8</sup>, E. Nagy<sup>6p</sup>), J. Nassalski<sup>15q</sup>), T. Niinikoski<sup>2</sup>, P.R. Norton<sup>11</sup>, F.G. Oakham<sup>11r</sup>), R.F. Oppenheim<sup>17s</sup>), A.M. Osborne<sup>2</sup>, V. Papavassiliou<sup>17</sup>, N. Pavel<sup>16t</sup>), C. Peroni<sup>13</sup>, H. Peschel<sup>16u</sup>), R. Piegaia<sup>17f</sup>), B. Pietrzyk<sup>8</sup>, U. Pietrzyk<sup>16v</sup>), B. Povh<sup>4</sup>, P. Renton<sup>10</sup>, J.M. Rieubland<sup>2</sup>, K. Rith<sup>4</sup>, E. Rondio<sup>15a</sup>), L. Ropelewski<sup>15a</sup>), D. Salmon<sup>12k</sup>), A. Sandacz<sup>15q</sup>), T. Schröder<sup>3</sup>, K.P. Schüller<sup>17</sup>, K. Schultze<sup>1</sup>, T.-A. Shibata<sup>4</sup>, T. Sloan<sup>5</sup>, A. Staiano<sup>13</sup>, H.E. Stier<sup>3</sup>, J. Stock<sup>3</sup>, G.N. Taylor<sup>10w</sup>), J.C. Thompson<sup>11</sup>, T. Walcher<sup>4l</sup>), J. Toth<sup>6p</sup>), L. Urban<sup>1</sup>, L. Urban<sup>6p</sup>), W. Wallucks<sup>3</sup>, S. Wheeler<sup>12k</sup>), W.S.C. Williams<sup>10</sup>, S.J. Wimpenny<sup>7x</sup>), R. Windmolders<sup>9</sup>, J. Womersley<sup>10y</sup>), K. Ziemons<sup>1</sup>,

*(Submitted to Zeitschrift für Physik)***ABSTRACT**

Differential multiplicities of forward produced hadrons in deep inelastic muon scattering on nuclear targets have been compared with those from deuterium. The ratios are observed to increase towards unity as the virtual photon energy increases with no significant dependence on the other muon kinematic variables. The hadron transverse momentum distribution is observed to be broadened in nuclear targets. The dependence on the remaining hadron variables is investigated and the results are discussed in the framework of intranuclear interaction models and in the context of the EMC effect.

- 
- a) University of Warsaw, Poland, partly supported by CPBP.01.06.
  - b) Permanent address, University of Bielefeld, Bielefeld, Germany.
  - c) Now at TRASYS, 1040 Brussels, Belgium.
  - d) Now at NIKHEF-K, 1009 AJ Amsterdam, The Netherlands.
  - e) Now at TESA S.A., Renens, Switzerland.
  - f) Now at City University, 1428 Buenos Aires, Argentina.
  - g) Now at University of Colorado, Boulder, Colorado, USA.
  - h) Now at British Telecom, London, UK.
  - i) Now at Jet, Joint Undertaking, Abingdon, UK.
  - j) Now at CERN, 1211 Geneva, Switzerland.
  - k) Now at R.A.L., Chilton, Didcot, UK.
  - l) Now at University of Mainz, 6500 Mainz, Germany.
  - m) Now at L.A.L., Orsay, France.
  - n) Now at University of California, Santa Cruz, CA 950-64, USA.
  - o) Now at RCNP, Osaka University, Ibaraki, Osaka 567, Japan.
  - p) Permanent address, Central Research Institute for Physics, Hungarian Academy of Science, 125 Budapest, Hungary.
  - q) Institute for Nuclear Studies, Warsaw, Poland, partly supported by CPBP.01.09.
  - r) Now at NRC, Ottawa, Canada.
  - s) Now at AT&T, Bell Laboratories, Naperville, Illinois, USA.
  - t) Now at DESY and University of Hamburg, II Institute of Experimental Physics, Germany.
  - u) Now at Gruner & Jahr, Itzehoe, Germany.
  - v) Now at MPI for Neurologische Forschung, Köln, Germany.
  - w) Now at University of Melbourne, Parkville, Victoria, Australia.
  - x) Now at University of California, Riverside, USA.
  - y) Now at University of Florida, Gainesville, USA.

### **Addresses**

- 1) III Physikalisches Institut A, Physikzentrum, RWTH, 5100 Aachen, Germany.
- 2) CERN, 1211 Geneva 23, Switzerland.
- 3) Fakultät für Physik, Universität Freiburg, 7800 Freiburg, Germany.
- 4) Max-Planck Institute for Kernphysik, 6900 Heidelberg, Germany.
- 5) Department of Physics, University of Lancaster, Lancaster LA1 4YB, UK.
- 6) Laboratoire d'Annecy-le-Vieux de Physique des Particules, B.P. 110, 74941, Annecy-le-Vieux, Cedex, France.
- 7) Department of Physics, University of Liverpool, Liverpool L69 3BX, UK.
- 8) Centre de Physique des Particules, Faculté des Sciences de Luminy, 13288 Marseille, France.
- 9) Faculté des Sciences, Université de Mons, 7000 Mons, Belgium.
- 10) Nuclear Physics Laboratory, University of Oxford, Oxford OX1 3RH, UK.
- 11) Rutherford and Appleton Laboratory, Chilton, Didcot OX1 0QX, UK.
- 12) Department of Physics, University of Sheffield, Sheffield S3 7RH, UK.
- 13) Istituto di Fisica, Università di Torino, 10125, Italy.
- 14) Department of Radiation Science, University of Uppsala, 75121 Uppsala, Sweden.
- 15) Physics Institute, University of Warsaw and Institute for Nuclear Studies, 00681 Warsaw, Poland.
- 16) Fachbereich Physik, Universität Wuppertal, 5600 Wuppertal, Germany.
- 17) Physics Department, Yale University, New Haven, Connecticut, U.S.A.

## I. INTRODUCTION

Deep inelastic lepton nucleus scattering offers a direct way to study the internal structure of the nucleus [1,2] as well as the hadronisation process which follows the hard scattering on partons [3]. In this process the target is probed with point-like particles whereas in hadron scattering, where the projectile itself has an internal structure, the situation is more involved. Moreover, in electron and muon experiments the incoming and scattered leptons are detected and they provide a well defined reference for the measurement of the kinematical variables of the hadrons.

Prior to the discovery of the EMC effect it was generally assumed that nuclear effects can be neglected at the high energy scale probed in deep inelastic scattering and so the nucleus can be regarded as a relatively loose conglomeration of nucleons. Any changes in the distribution of the final state hadrons from different nuclear targets could be ascribed to absorption effects inside the nucleus. It was hoped that the study of these absorption effects at different beam energies and with different targets would yield information about the space time structure of the hadron jet formed in deep inelastic processes [4,5].

The discovery of the EMC effect [6] has shown that this simple picture has to be modified. Many models have been developed to explain this effect, but none of them are able to describe the  $x$ -dependence of the  $F_2$  ratio in the full  $x$  range (for a review see [7]).

It is important to investigate whether the nuclear environment also influences the hadronisation process. Moreover, the hadron analysis offers a new way to study the problem of the EMC effect independently from the structure function analysis. This may help to discriminate between the large number of possible models.

While a lot of experimental data on hadron nucleus scattering have been compiled (e.g. [8-11]), in only a few lepton nucleus scattering experiments the hadron distributions have been analysed [13,36]. In this paper, new more precise data on muon scattering in heavy targets over a wider kinematic range than before are presented. The scattered muon and the fast hadrons from the different targets were measured using a target arrangement designed to minimise any systematic errors due to time dependent effects in the efficiency or the acceptance of the apparatus.

## II. THE EXPERIMENT

The experiment was performed in the M2 muon beam line at the CERN SPS using the EMC forward spectrometer to detect the scattered muon and the fast hadrons. Figure 1a) shows a schematic diagram of the apparatus which is similar to that described in [14] with certain modifications to improve the efficiency of the apparatus in the beam region and to allow data to

be taken at higher intensities than previously achieved. In scattering experiments with extended heavy targets, high track multiplicities, due to low energy electrons from photon conversion and hadrons from secondary interaction in the target, are to be expected. Therefore, the drift chambers in front of the magnet in the original setup [14] were replaced by multiwire proportional chambers labelled PV1 and PV2. Small proportional chambers designed to operate in a high intensity environment (POB, POD, POE) were installed to measure tracks in the desensitised central parts of PV1, PV2. As the reconstruction of hadrons starts with hits in the large drift chambers in front of the hadron absorber (W4 and W5), it was decided to cover the central region of these detectors by additional multiwire proportional chambers (P4 and P5).

Two different target arrangements were used for the measurements with heavy targets. In 1984, at the same time as the measurement of the spin dependent structure functions with a polarised  $\text{NH}_3$  target [12,15], several heavy targets were exposed to the beam. The arrangement, shown in fig.1b), consisted of a 50 cm long deuterium target and also carbon, copper and tin targets of comparable thickness (about  $8 \text{ g/cm}^2$ ) suspended from a movable boom which allowed frequent target changes. The solid targets were each cut in 4 thin slices and distributed over the same region in space as the deuterium target cell so that the acceptance from each was the same.

In 1985 the polarised target was replaced by an extended deuterium/copper target to make a higher precision comparison. Two 1 m long deuterium tanks and five copper slices of different thickness in a sandwich-like arrangement (see fig.1c), were simultaneously exposed to the beam in such a way that the differences in acceptance between the individual parts of the targets averaged out.

The data used for the analysis presented here were taken with both target configurations in several experimental runs with incident muon energies of 100, 120, 200 and 280 GeV.

### III. DATA ANALYSIS

The standard variables in deep inelastic scattering, as defined in table 1, are used in this paper. Figure 2 illustrates the definition of the hadron variables which will be investigated here;  $z_h$  is the fraction of the virtual photon energy carried by the hadron ( $z_h = E_{\text{had}} / \nu$  with  $E_{\text{had}}$  the hadron energy in the laboratory system),  $p_{\perp}$  is the component of the momentum of the hadron transverse to the virtual photon direction and  $\varphi$  the azimuthal angle of the hadron around the direction of the virtual photon.

The data were processed through a chain of analysis programs which performed pattern recognition and reconstruction of tracks and interaction vertices. A fit for the primary vertex was made using the incident and scattered muon tracks. An attempt was then made to associate

the other tracks with the primary vertex, whose position was improved to optimise the  $\chi^2$  for the fit.

To exclude kinematic regions with small or rapidly varying acceptance for both the muons and hadrons the cuts listed in table 2 were applied.

The influence of bremsstrahlung on the hadron spectra is included in the Monte Carlo simulation of the acceptance. Final state hadrons were generated using the Lund string model [16] taking into account the QED radiative processes. All outgoing particles, including the scattered muon and radiative photon, were tracked through the target and the apparatus. The procedure used included the effects of secondary interactions in the target, photon conversions and multiple Coulomb scattering. The effects of the detector inefficiencies and kinematical smearing were also included and the simulated track coordinates in each chamber measurement were passed through the data analysis program chain. The raw data ratios of hadron multiplicities, normalised by the number of scattered muons, were corrected using the factors obtained from this detailed Monte Carlo simulation.

The multiplicities obtained from the Monte Carlo simulation were 0.5 - 5% higher than the measured ones. These differences are probably due to an incomplete simulation of track losses in the vertex fit and cancel out when ratios of multiplicities from different targets are taken. The corrections applied to the multiplicity ratios deviate by only a small amount from unity (typically 3 - 5%) except for regions where the contribution of the coherent tail from radiative processes is high. The emission of a very hard photon mimics a deep inelastic event with no hadron observed, and this effect is corrected for. The cuts in x and y (see table 2) are chosen to limit these corrections to be everywhere less than 10%.

A calorimeter (labelled H2 in fig.1), consisting of an electromagnetic part of 20 radiation lengths thickness followed by a hadronic part with 3.5 interaction lengths of active material, was used to identify electrons. For a charged particle to be classified as an electron it was required that the relative fraction of the particle's measured energy, deposited in the electromagnetic part, was greater than 80%. The overall efficiency for removing electrons by this cut, outside a circle of 12 cm radius around the beam hole of H2, was found to be  $94 \pm 4\%$  and  $90 \pm 7\%$  for runs with a beam energy of 100 and 280 GeV respectively. The fraction of hadrons, which were misidentified as electrons by this method, was determined to be between 7-9%. The measured ratios have been corrected for both these effects.

The numbers of events, which passed these event selection criteria, are listed separately in table 3 for the different targets and beam energies.

#### IV. SYSTEMATIC ERRORS

A list of uncertainties, which contribute to the systematic error of the multiplicity ratios, is given in table 4. A detailed discussion of the studies of these systematic errors can be found in [17, 18]. In this experiment most of the systematic errors cancel in taking the ratios since both targets were simultaneously exposed to the beam.

The largest error comes from the correction for the electron contamination of the hadron distributions, which has been described in the previous section. These errors, however, almost cancel when taking ratios of distributions from different targets (as discussed above), so that this systematic error is nearly always smaller than the statistical error. The radiative correction is different for each target at low  $x$  and high  $y$  due to the coherent and quasielastic radiative tail. Within the kinematic cuts given in table 2 the systematic uncertainty due to the radiative corrections is less than 1% ([18] and references therein).

As the apparatus and geometrical efficiency were the same for each of the two targets being compared and the shape of the hadron distributions from different targets are very similar, systematic errors in the measurement of the muon or hadron momentum do not significantly affect the measured ratios. For the same reason the influence of systematic errors due to the track selection and the apparatus efficiency is negligible. Furthermore, the loss of events or tracks due to the finite software reconstruction efficiency is the same for all targets and does not affect the measurement of hadron distribution ratios.

The quality of the Monte Carlo simulation of the secondary interactions in the target was checked by comparing the results from the upstream and the downstream parts of the target. No systematic trend could be found and the uncertainties are less than the statistical errors except for the very low  $v$ -region, where they are comparable.

The errors shown in the data presented always include the systematic error from the correction for the electron contamination (added in quadrature to the statistical error). The magnitude of the remaining error, not shown in the figures, is less than 1%.

#### V. RESULTS

The distributions in  $z$  and  $p_{\perp}$  and the azimuthal asymmetry of the charged hadrons in the forward hemisphere have been investigated to search for nuclear effects in the hadron jets. The ratio of the numbers of positively and negatively charged hadrons from nuclear targets have been compared to those from deuterium and these allow limits to be set on any excess contribution of sea quarks in the nucleus.

## V.1 $z_h$ Distributions of Charged Hadrons

The  $z$  distribution of charged hadrons normalised to the number of scattered muons and integrated over the muon variables within the cuts given in table 2, is shown in fig. 3 separately for copper and deuterium. Figure 4 shows the ratio of the differential multiplicity distributions  $r_{Cu}(z_h)$  as a function of  $z_h$  for copper and deuterium, where

$$r_{Cu}(z_h) = \left( \frac{1}{N_\mu} \frac{dN^h}{dz_h} \right)_{Cu} / \left( \frac{1}{N_\mu} \frac{dN^h}{dz_h} \right)_{D_2}, \quad (5.1)$$

together with the ratios measured using the carbon and the tin targets.

For the large nuclei (Cu, Sn) one observes a small but distinct reduction of the fast hadron production compared to that on deuterium, whereas for carbon the ratio is compatible with unity over the whole range in  $z_h$ . The high statistics experiment with Cu and  $D_2$  reveals that there is no significant variation of the ratio for  $z_h > 0.2$ . For smaller  $z_h$  the ratio tends to rise to a value greater than unity. A similar trend can also be seen for Sn. The averaged multiplicity ratios for  $z_h > 0.2$  defined as

$$R_A = \left( \int_{0.2}^1 dz_h \frac{dN^h}{dz_h} \right)_A / \left( \int_{0.2}^1 dz_h \frac{dN^h}{dz_h} \right)_{D_2} \quad (5.2)$$

are given in table 5. The observed depletion of hadrons is significantly more pronounced for heavy nuclei than for lighter ones.

The higher statistics of the Cu and  $D_2$  data allow further studies of the dependence of  $R_{Cu}$  on the muon variables. In fig. 5 the ratio  $R_{Cu}$  is plotted versus  $\nu$  in the range from 10 to 230 GeV. The ratios show a gradual decrease with decreasing  $\nu$  below  $\nu \leq 60$  GeV, whereas they slowly approach unity for higher  $\nu$ . It should be noted, that the depletion of the fast hadron multiplicity in copper, even in the lowest  $\nu$ -bin, is only  $\approx 10\%$ .

Our data, taken at two beam energies, allow the dependence of  $R_{Cu}$  on the muon variables to be investigated. In fig. 6 the ratio of the partial integrals  $R_{Cu}$  is plotted as a function of  $\nu$  for several bins in  $Q^2$  and  $x$ . The same characteristic variation with  $\nu$  can be seen in all intervals. If one separates off the  $\nu$ -dependence by an unfolding procedure, no trend in  $Q^2$  nor in  $x$  can be observed [18].

Thus, the data are consistent with the variation of the hadron multiplicity being in the variable  $\nu$  alone.

## V.2 $p_{\perp}$ Distributions

An anomalous A-dependence of the single particle  $p_{\perp}^2$ -spectra was observed in hadron nucleus experiments [19] and induced considerable theoretical activity in the field of initial state interactions. Also the strong enhancement of the mean value of  $p_{\perp}^2$  in the production of massive muon pairs by the Drell Yan process [20] is attributed to such effects [21,22]. In lepton nucleus collisions neither multiple scattering of the incident particle nor interaction of its constituents complicate the interpretation. Hence the residual nuclear effects can be studied directly.

The ratio of  $p_{\perp}^2$ -spectra for Cu/D<sub>2</sub> is displayed in fig. 7 for two  $\nu$ -intervals. In the lower  $\nu$ -bin one finds a small depletion of hadrons for Cu relative to D<sub>2</sub>, which reflects the  $\nu$ -dependence described in the previous subsection. At high  $p_{\perp}^2$  the ratio  $r_A(p_{\perp}^2)$  rises above unity in both  $\nu$  intervals. At high  $\nu$  the maximum variation of  $r_{Cu}(p_{\perp}^2)$  is about 0.2. In the proton collisions [19] the ratio in the same  $p_{\perp}^2$  interval varies by 0.5. Therefore the observed effect in deep inelastic muon scattering has the same trend but is smaller in magnitude.

The nuclear effects on the  $p_{\perp}^2$ -distributions can be further analysed in terms of the average  $p_{\perp}^2$  ratios from Cu and D<sub>2</sub> targets. This quantity is sensitive to differences in the slopes and the tails of the distributions at high  $p_{\perp}^2$ . Figure 8 shows the ratio of the average values of  $p_{\perp}^2$  for hadrons from copper to those from deuterium as a function of  $\nu$ . At low  $\nu$  the ratio is larger than unity by a few percent, whereas at high  $\nu$  it becomes compatible with unity. We have also checked that this ratio shows no significant dependence on  $z_h$  [18]. This demonstrates that at high  $\nu$  the 'seagull' effect in  $\mu$ -nucleus scattering is of the same size as in the  $\mu$ -p process (no difference between  $\mu$ -D<sub>2</sub> and  $\mu$ -p scattering was found in  $p_{\perp}^2$ -distributions [23]). Both the  $\nu$  and  $z_h$  dependences support the hypothesis that rescattering in the final state is the source of the observed enhanced average transverse momentum of the hadrons.

## V.3 Azimuthal Angle Asymmetry

The distributions of the azimuthal angle,  $\phi$  (see fig.2) of the fast forward hadrons has been investigated. In  $\mu$ -p scattering a clear deviation from an isotropic  $\phi$ -distribution has been measured previously [24-26]. Figure 9 shows that a similar effect is also observed in the data from Cu and D<sub>2</sub>.

To quantify the asymmetry measurement the distribution of the normalised differential hadron multiplicities  $1/N^h * dN^h / d\phi$  are fitted by a function of the type  $a_1 + a_2 \cos(\phi)$  (full and dashed lines in fig. 9 for Cu and D<sub>2</sub>, respectively) suggested by theoretical consideration [27-30]. The mean value of  $\cos(\phi)$  can be easily expressed by the coefficients of the fit:



$$\langle \cos(\varphi) \rangle = \int_0^{2\pi} d\varphi f(\varphi) \cos(\varphi) / \int_0^{2\pi} d\varphi f(\varphi) = a_2 / 2a_1 \quad (5.3)$$

The possibility of a  $\cos(2\varphi)$  and a  $\sin(\varphi)$  term has also been considered. However, it has been shown that these terms are small and that the value of  $\langle \cos(\varphi) \rangle$  does not change significantly if they are neglected [24]. It is important to note that this asymmetry parameter is independent of the absolute normalisation of the hadron distributions; the distribution in fig. 9 is therefore arbitrarily normalised to  $2\pi$ .

The results of the  $\varphi$ -moment analysis performed, in two bins of  $W^2$  and three bins in  $z_h$ , are given in fig. 10. Here  $W$  is the energy in the virtual photon-proton rest frame. The values obtained from the copper and deuterium targets are equal within errors and they agree with previous measurements on  $H_2$  [24,25].

For a precise comparison of the  $\varphi$  asymmetries on different targets the ratio of  $\varphi$ -distributions,  $r(\varphi)$ , on two different targets has been studied, where:

$$r(\varphi) = (1 + \kappa \cos(\varphi)) / (1 + \delta \cos(\varphi)) \approx 1 + \Delta \cos(\varphi)$$

$$\text{with } \Delta = \kappa - \delta \text{ and } \kappa = 2 \langle \cos(\varphi) \rangle_{\text{Cu}}; \quad \delta = 2 \langle \cos(\varphi) \rangle_{\text{D}_2} \quad (5.4)$$

The dependence of  $r(\varphi)$  is shown in fig.11 for the high  $z$  and  $v$  bin, where the asymmetry for each target is the biggest. Thus, from the asymmetry of the ratio  $r(\varphi)$  of the  $\varphi$  distributions the difference  $\Delta$  of the asymmetry in Cu and  $D_2$  can be directly determined with the highest possible precision. The quantity  $\Delta$  is compatible with zero over the whole kinematical range explored. This result is discussed in more detail below.

## VI. DISCUSSION

Lepton nucleus scattering is simpler than high energy hadron nucleus or heavy ion collisions. It can be described by a 3-step process: the hard scattering of the virtual photon and a parton, the hadronisation of the outgoing partons and the possible reinteraction of either the quarks, before being confined, or the final state hadrons. This can be expressed in the following compact ansatz for the semi-inclusive cross section:

$$\frac{1}{\sigma_{\text{tot}}} \frac{d\sigma}{dx_h} = \left\{ \sum_i e_i^2 q_i(x, Q^2) D_q^h(z_h, P_{\perp}, \varphi, Q^2, x) / \sum_i e_i^2 q_i(x, Q^2) \right\} \alpha_{\text{reint}}(z_h, P_{\perp}, v) \quad (6.1)$$

where  $q_i(x, Q^2)$  = quark distribution function,  $e_i$  = charge of quark  
 $D_q^h$  = fragmentation function  
 $x_h$  = one of the hadronic variables  $z_h$ ,  $p_\perp$  or  $\phi$  defined in fig. 2.

The term,  $\alpha_{\text{reint}}(z_h, p_\perp, \nu)$  describes possible effects of the final state interaction inside the nucleus. In section VI.1, below, the results of the hadron multiplicity ratios are interpreted in terms of different models for intranuclear reinteraction.

Since the discovery of the EMC effect, the possible nuclear dependence in the effective quark densities on hadron production must be taken into account. The question as to whether there is a change in the fragmentation process in a nuclear environment, which would affect the hadron distributions, is addressed in section VI.2. The understanding of nuclear effects in the hadronic final state can, furthermore, help to find the interpretation of the EMC effect in a way which is independent of the structure function ( $F_2$ ) analysis. The  $A$  and  $x$  dependences of the  $F_2$  ratios have been measured in deep inelastic scattering and in the Drell Yan process [31]. These experimental facts are faced with a plethora of theoretical models describing the effect. In the last section we discuss how further constraints on these models can be obtained from the hadron analysis.

### VI.1 Models for Intranuclear Interactions

It has been appreciated for a long time that information on the space time structure of the hadronisation process and on the behaviour of a non-confined quark in nuclear matter can be extracted from the analysis of the hadrons produced in lepton nucleus scattering. In particular the study of the energy dependence of hadron multiplicity ratios can be used in this context [32,33].

Previously experiments have been performed only at lower energy [34-38]. In all but one [36], only the total charged hadron multiplicity  $\langle n \rangle$  was determined. Despite sizable statistical and systematic errors an increase of  $\langle n \rangle$  in nuclei was seen. In [36] a strong suppression of the fast hadron production, increasing with the size of the target nucleus was observed. Both facts were interpreted as an indication for intranuclear cascading [4,33]. At higher energies a suppression of the fast hadrons was also observed [13].

The models existing at that time were based on the bremsstrahlung analogy [39]. They contained two independent and a priori unknown parameters, namely the scale for the hadron formation time  $\tau_h$  and the quark cross section  $\sigma_q$ . For the calculation of ratios of the hadron multiplicities from a nuclear and a free proton target the nuclear density function is folded with the probability that a quark or a hadron exists inside the nucleus. This can be expressed in a general ansatz [33]:

$$R_A = 2\pi \int_0^\infty b db \int_{-\infty}^{+\infty} dx \rho(b,x) \left[ 1 - \sigma_q \int_x^\infty dx' \rho(b,x') P_q(x'-x) - \sigma_h \int_x^\infty dx' \rho(b,x') P_h(x'-x) \right]^{A-1} \quad (6.2)$$

- $\rho(b,x)$  = nuclear density function:  $b$  = impact parameter;  
 $\sigma_q(\sigma_h)$  = cross section for quark (hadron) reinteraction;  
 $P_q(P_h)$  = probability that a quark (hadron) exists at a distance  $x' - x_0$   
 from the point of the photon-parton interaction at  $x_0$ .

The hadronic interaction cross section is usually taken to be  $\sigma_h \approx 20$  mb.

In the first models proposed [4,5,33]  $P_q$  and  $P_h$  depend on the formation time  $\tau_h$ , of either the hadron or the struck quark (i.e.  $\nu$ ), which is assumed to grow with the energy due to Lorentz dilatation. Thus the nuclear absorption effect was expected to die out at higher energies. However, it was completely unknown at which energy this would occur.

The new data available from this analysis allow for the first time, a wide range in  $\nu$  to be explored with high accuracy. It was ascertained in section V.I that the energy  $\nu$  is indeed the relevant variable on which the ratio of hadron multiplicities depends. As the kinematic ranges covered by the SLAC and the EMC experiment have little overlap the EMC data sets have been combined in order to investigate further the  $\nu$ -dependence.

Figure 12a shows the measured ratios of the integrals of the hadron multiplicities, defined in section V.1 (eq. 5.1) and as a function of  $\nu$ , together with predictions of the theoretical models. The dotted line (curve 1) represents the prediction of a calculation using the bremsstrahlung analogue ansatz of [4,5,33]. The hadron formation time  $\tau_h$  is the only time in this ansatz. For this calculation  $\tau_h$  has been assumed to be proportional to the hadron's energy ( $\tau_h = z_h \nu$ ) and the quark reinteraction cross section  $\sigma_q$  has been set to zero. There is a significant discrepancy between the shape of the model curve and the observed  $\nu$ -dependence using the combined results of [36] and this analysis. A finite value for  $\sigma_q$  would yield an even weaker variation with  $\nu$ . The older results of [13] are consistent with this model within the errors. However, the new data at high  $\nu$  show that with any choice of the parameters  $\sigma_q$  and  $\tau_h$  only a poor description of the energy dependence of the nuclear absorption effect can be achieved with these models.

The above models are oversimplified as hadrons are composite objects. It is not, a priori, evident in which state of the hadron formation the interaction with the environment starts. Recently, Bialas and Gyulassy [40] proposed to calculate the probabilities  $P_q$  and  $P_h$  using the space time structure of the fragmentation process from the Lund string model. In this context the formula (6.2) has to be modified:

$$R_A = 2\pi \int_0^\infty b db \int_{-\infty}^\infty dx \rho(b,x) \left[ 1 - \sigma^* \int_x^{\tau_c} \rho(b,x') dx' - \sigma_s \int_{\tau_c}^{\tau_h} \rho(b,x') dx' - \sigma_h \int_{\tau_h}^\infty \rho(b,x') dx' \right]^{A-1} \quad (6.2')$$

where  $\sigma_s$  is the cross section for the interaction of the open string (which becomes one of the hadron quarks being looked at).

These authors derived a relationship between the energy of the hadron (i.e.  $z_h$  and  $v$ ) and the time,  $\tau_c$ , at which its constituent appears after the photon parton scattering (see fig.12b). The difference between  $\tau_h$  and  $\tau_c$  is given by the simple formula:  $\tau_h - \tau_c = z_h v / \kappa$ , where  $\kappa$  is the string tension. This model contains two time scales for the hadron formation process. It should be noted that the predicted value of  $\tau_c$  is greater than zero (apart from the extreme  $z_h$  ranges,  $z_h \rightarrow 1$  and  $z_h \rightarrow 0$ ), and that this result is independent of the details of the string model; the only free parameter is  $\kappa$  ( $\approx 1$  GeV/fm).

With this ansatz one can reproduce the characteristic energy dependence in a much better way (full line (curve 3) in fig.12a) [18,41]. In contrast to the one scale model it is necessary to introduce a sizable cross section for the interaction of an open string  $\sigma_s$  (to be compared with the dashed curve). Here it is assumed that no reinteraction occurs before the constituent quark has appeared ( $\sigma^* = 0$  mb). The agreement of data and model calculation can be improved, if one admits a small interaction probability from the time of the photon parton collision [42] (i.e.  $\sigma^* \approx 0.75$  mb, dashed dotted line (curve 4) in fig.12a).

In the context of these models the results show that the unconfined (undressed) quark (or colour string) strongly interacts with nuclear matter, and that reinteractions occur a long time before the formation of final hadrons. This information may have interesting implications for the interpretation of the more complex reaction like hadron nucleus and heavy ion collisions.

## VI.2 Hadron Production and Models for the EMC Effect

Before the discovery of the EMC effect final state interactions were the only source of nuclear effects to be considered for hadron distributions. It has now become evident that the interpretation is more complex and an interplay of different effects is possible, leading to the observed small nuclear effects.

The nuclear effects on the structure function of the nucleon are most frequently attributed to a change in the effective quark distribution functions. Calculations, in which the nuclear dependence of the quark distribution has been considered, show that the effect on the ratios of the sum of charged hadrons ( $N^{h+} + N^{h-}$ ) is of the order of a few tenths of a per cent, and hence

negligible [18]. The absence of any substantial impact of the EMC effect on the ratio of the sum of charged hadrons ( $N^+ + N^-$ ) is an important a posteriori justification for the hadron analysis discussed in the preceding subsection.

On the other hand, the ratio of the positive to negative hadrons  $N^{h+} / N^{h-}$  is sensitive to modifications of the sea quark distributions. From a study of the double ratio  $R_{+-} = (N^{h+} / N^{h-})_{Cu} / (N^{h+} / N^{h-})_{D_2}$  one can extract limits on the possible change of the sea in Cu compared to  $D_2$ . Here  $N$  represents the partial integrals from  $z_h = 0.2$  to 1.0 defined in section V.1 with superscript  $+(-)$  referring to positive (negative) tracks. In the  $x$  interval  $0.02 < x < 0.08$ , where the fractional momentum carried by sea quarks amounts to about 50%, the double ratio  $R_{+-}$  of the partial integrals is found to be  $1.006 \pm 0.025$ , where a correction for the non-isoscalarity of Cu ( $\approx 0.01$ ) has been applied. Using a simple quark parton model calculation the ratio of the fractional momentum carried by the sea in Cu and  $D_2$  is  $0.97 \pm 0.10$ . This result implies an upper limit of 26% for the change of the fractional momentum carried by the sea (at 90% c.l.) between copper and deuterium. Some of the models, which predict a nuclear dependence of the sea [43,44] are not compatible with this measurement.

It is also possible to examine the effects of the nuclear medium on the fragmentation functions. In [45] it is suggested that the fragmentation function may rescale by analogy with the structure function  $F_2$ , thus:

$$D_q^h(z_h, Q^2) \Big|_A = D_q^h(z_h, \xi Q^2) \Big|_{A_0} \quad A_0 < A; \xi > 1. \quad (6.3)$$

In fig. 13 the measured ratio of differential hadron multiplicities for Cu/ $D_2$  data, restricted to low  $v$  with an average value of 35 GeV, is compared to calculations using this ansatz with various rescaling parameters  $\xi$ . At this value of  $v$  the formation length of most of the hadrons is predicted to be about 1-2 times larger than the radius of the copper nucleus [33,40], so that a significant part of the hadronisation process takes place inside the nucleus. Thus a possible influence of the nuclear environment on the fragmentation can be studied. The dotted line is obtained, with the value of  $\xi$  equal to the ratio of the confinement radius  $r_{cf}$  in Cu and  $D_2$ , as deduced by fitting the EMC structure function ratio [46]. If one uses an analogy with the  $F_2$  rescaling scheme the corresponding rescaling parameter for  $F_2$  ( $\xi = r_{cf,Cu} / r_{cf,D_2} \alpha_s(Q^2) / \alpha_s(\mu^2) = 2.02$ ), the model curve (dashed line) does not reproduce the shape of the  $z_h$  distribution ratio in a satisfactory way. This shows that moderate rescaling ( $\xi \leq 1.3$ ) cannot be excluded, but that significantly higher rescaling parameters, as for example proposed in [47], would not be compatible with these measurements.

Another interesting idea is that of Nachtmann and Pirner [48] who predict a harder fragmentation function in a nuclear environment. No quantitative details are given in the publication. However, because of isospin invariance it is reasonable to assume that the energy is distributed among charged and neutral particles in a nuclear independent manner. Therefore,

a harder fragmentation function in  $\mu$  - Cu scattering would make the ratio of  $z$  distributions look like the full line in fig. 13. For this calculation, the parameterisation of the pion fragmentation function, measured by the EMC on a  $D_2$  target [49], was used:  $D_{\mu}^+ = b * (1 - z_h)^\epsilon$ . For the Cu target both the exponent  $\epsilon$  has been lowered by 2.5% and the parameter  $b$  adjusted, so that the total energy is conserved. Figure 13 shows that, independent of the absolute size of the effect, the prediction is in clear contradiction with the data. It has been shown that these conclusions remain valid [18] even when intranuclear cascading effects are taken into account.

Many models explain the EMC effect by postulating that the confinement radius of a quark in a bound nucleon is larger than that in a free nucleon [47,50-52]. By the uncertainty principle, this implies a reduction of the mean transverse momentum,  $\langle k_{\perp} \rangle$  of a quark in a bound nucleon. It has been demonstrated that the  $\phi$  asymmetry is proportional to the value of  $\langle k_{\perp} \rangle$  [53,24]. Hence a difference in the  $\phi$  asymmetry in bound and free nucleons can be used to infer a difference in  $\langle k_{\perp} \rangle$  and hence in the quark confinement radius. The high  $z_h$  and high  $\nu$  region is most sensitive to this effect. Figure 14 shows the value of  $\langle \cos\phi \rangle$  versus  $\langle k_{\perp} \rangle$  for  $z_h > 0.4$  and  $\langle \nu \rangle = 145$  GeV as determined from the model of [53]. In this region the difference in the value of  $\langle \cos\phi \rangle$  between copper and deuterium is measured to be  $-0.014 \pm 0.023$  from a fit to the data in fig. 11. From the slope of the calculated line in fig. 14, the difference between the value of  $\langle k_{\perp} \rangle$  in copper and that in deuterium is inferred to be less than 0.2 GeV (at 90% confidence level). Taking the value  $\langle k_{\perp} \rangle = 0.7$  GeV in a free nucleon [25], this implies that the confinement radius in nucleons bound in copper is not more than 30% (90% c.l.) larger than that of quasi free nucleons in deuterium.

## VII. CONCLUSIONS

Final state hadron distributions in deep inelastic muon scattering on heavy targets have been compared with those in  $\mu$ - $D_2$  scattering. The systematic errors for ratios of the hadron multiplicities are small compared to the statistical errors. This was ensured by making measurements simultaneously with a deuterium target and one of the heavy targets.

The nuclear effects in the energy range explored here are generally rather small. Integrated over the muon kinematic variables the ratio of the fast forward produced hadrons ( $z_h \geq 0.2$ ) produced on Cu with respect to those produced on  $D_2$  is  $0.946 \pm 0.008$  (stat)  $\pm 0.005$  (syst), at an average  $\nu$  of 62 GeV. This ratio is somewhat lower for tin and compatible with unity for carbon. No dependence of this quantity on  $Q^2$  or  $x$  has been found, but a significant variation with  $\nu$  is demonstrated. The multiplicity suppression is strongest in the lowest  $\nu$  bin and disappears in the highest  $\nu$ -interval.

The ratio of  $p_{\perp}^2$ -distribution of Cu/D<sub>2</sub> rises to values above unity for  $p_{\perp}^2 \geq 1 \text{ GeV}^2/c^2$ . This effect is similar to that observed in the hadron nucleus scattering, but is smaller in magnitude.

The new precise data from this analysis covering a wide range in  $v$ , in combination with the results of an electron scattering experiment at low energy at SLAC, allow discrimination between different models for final state particle interaction. The older models, based on the bremsstrahlung analogy, fail to describe the characteristic energy dependence of the hadron depletion. A model recently developed by Bialas and Gyulassy, which involves a finite formation time for both the final states hadrons and the constituent quarks, has been applied to the deep inelastic scattering process. The data can be described much better by this model, but only with the assumption that the constituent quarks have a sizable cross section to interact with the nuclear matter. These results support the picture of the space time structure in the Lund string fragmentation model and indicate that the reinteraction with nuclear matter starts a long time before the formation of the final state hadrons.

The relationship between the hadron production in  $\mu$ -nucleus scattering and the EMC effect has been investigated. By comparing the ratio of positive to negative hadrons a 90% c.l. upper limit of 26%, for a possible change of the sea quark contribution in Cu compared to D<sub>2</sub>, has been set. The influence of a change in the quark densities on the charged summed hadron distributions is negligibly small.

No indication for a significant change of the fragmentation function in a nucleus has been found at larger values of  $v$ .

The difference of the azimuthal asymmetry of forward produced hadrons in  $\mu$ -Cu and  $\mu$ -D<sub>2</sub> scattering is compatible with zero and sets a limit for the difference of the confinement radius in Cu and D<sub>2</sub>. This excludes models for the EMC effect which postulate an increase of the confinement radius of more than 25%.

## References

- [1] EMC, J. Ashman et al., Phys. Lett. **B202** (1988) 603.
- [2] A. Bodek et al., Phys. Rev. Lett. **50** (1983) 1431;  
A. Bodek et al., Phys. Rev. Lett. **51** (1983) 543;  
R.G. Arnold et al., Phys. Rev. Lett. **52** (1984) 727;  
A.C. Benvenuti et al., Phys. Lett. **189B** (1987) 483.
- [3] EMC, M. Arneodo et al., Z. Phys. **C35** (1987) 417 and references therein.
- [4] N.N. Nikolaev, Z. Phys. **C5** (1980) 291.
- [5] A. Bialas, Acta Physica Polonica **B11** (1980) 475.
- [6] EMC, J.J. Aubert et al., Phys. Lett. **123B** (1983) 275.
- [7] L. Frankfurt and M. Strikman, Phys. Rep. **160** (1988) 235;  
E.L. Berger and F Coester, Ann. Rev. Nucl. and Particle Science **37** (1987) 463.
- [8] K. Abe et al., Phys. Lett. **200B** (1988) 266.
- [9] R. Gomez et al., Phys. Rev. **D35** (1987) 2736.
- [10] C. de Marzo et al., Phys. Rev.
- [11] J. E. Elias et al., Phys. Rev. **D22** (1980) 13.
- [12] EMC, J. Ashman et al., Phys. Lett. **B206** (1988) 364.
- [13] EMC, A. Arvidson et al., Nucl. Phys. **B246** (1984) 381
- [14] EMC, O.C. Alkofer et al., Nucl. Inst. and Meth. **179** (1981) 445.
- [15] EMC, J. Ashman et al., Nucl. Phys. **B328** (1989) 1.
- [16] B. Andersson et al., Phys. Rep. **97** (1983) 31;  
T. Sjöstrand, Phys. Lett. **142B** (1984) 420.
- [17] J. Womersley, 'A Study of Forward Hadron Production in Deep Inelastic Muon-Nucleus Scattering', Ph.D. thesis, Oxford (1986).
- [18] N. Pavel, 'Hadron Production in Deep Inelastic Muon Nucleus Scattering' Ph.D. thesis, Univ. of Wuppertal, WUB-DI 89-4 (1989).
- [19] J.W. Cronin et al., Phys. Rev. Lett. **31** (1973) 1426;  
D. Antreysan et al., Phys. Rev. **D19** (1979) 764.
- [20] P. Bordalo et al., Phys. Lett. **193B** (1987) 373.
- [21] C. Michael and G. Wilk, Z. Phys. **C10** (1981) 169.
- [22] G.T. Bodwin, S.J. Brodsky and G.P. Lepage, Phys. Rev. Lett. **47** (1981) 1799.
- [23] U.Krüner, Diploma thesis, Univ. of Wuppertal, WUB 89-5 (1989).
- [24] N. Pavel, Diploma thesis, Univ. of Wuppertal, WUB 83-7 (1983).
- [25] EMC, J.J. Aubert et al., Phys. Lett. **130B** (1983) 118.
- [26] EMC, M. Arneodo et al., Z. Phys. **C34** (1987) 277.
- [27] G.v.Gehlen, Nucl. Phys. **B26** (1971) 141.
- [28] R.N. Cahn, Phys. Lett. **78B** (1978) 269.



- [29] A. Mendez, Nucl. Phys. **B145** (1978) 199.
- [30] H. Georgie and H.D. Politzer, Phys. Lett. **40B** (1978) 3.
- [31] P. Bordalo et al., Phys. Lett. **193B** (1987) 368.
- [32] N.N. Nikolaev and G.V. Davidenko, Nucl. Phys. **B135** (1978) 333.
- [33] A. Bialas and T. Chmaj, Phys. Lett. **133B** (1983) 241.
- [34] T.H. Burnett et al., preprint Univ. of Washington/Seattle, VTL-PUB 44 (1977).
- [35] J.P. Berge et al., Phys. Rev. **D18** (1978) 3905.
- [36] L.S. Osborne et al., Phys. Lett. **40B** (1978) 1624.
- [37] L. Hand et al., Z. Phys. **C1** (1979) 139.
- [38] H. Deden et al., Nucl. Phys. **B198** (1982) 365.
- [39] L. Stodolsky, Proc. of 6th Int. Symposium on Multiparticle Dynamics, Oxford (1975).
- [40] A. Bialas and M. Gyulassy, Nucl. Phys. **B291** (1987) 793.
- [41] P. Renton Oxford University, Nucl. Phys. Lab., preprint 55-88;  
R. Windmolders, Proc. XXIV Int. Conf. on High Energy Physics,  
Munich (1988) p. 267.
- [42] A. Bialas and J. Czyzewski, preprint Univ. of Cracow, TPJU-16/88 (1988).
- [43] C.H. Llewellyn-Smith, Phys. Lett. **128B** (1983) 107.
- [44] M. Ericson and A.W. Thomas, Phys. Lett. **128B** (1983) 118.
- [45] J. Dias de Deus, Phys. Lett. **166B** (1986) 98.
- [46] F.E. Close et al., Phys. Rev. **D31** (1985) 1004.
- [47] O. Nachtmann and H.J. Pirner, Z. Phys. **C21** (1984) 277.
- [48] O. Nachtmann and H.J. Pirner, preprint Univ. of Heidelberg, HD-THEP 84-7 (1984).
- [49] EMC, J.J. Aubert et al., Phys. Lett. **160B** (1985) 417.
- [50] F.E. Close et al., Phys. Lett. **129B** (1983) 346.
- [51] R.L. Jaffe, Phys. Lett. **134B** (1984) 449.
- [52] H. Faissner et al., Phys. Rev. **D30** (1984) 900.
- [53] P. Kroll and A. Koenig, Z. Phys. **C16** (1982) 89.
- [54] N. Pavel, preprint Univ. of Wuppertal WUB 82-10 (1982).

Table 1: Definition of the muon kinematic variables in the laboratory frame	
$m$	Lepton rest mass
$M$	Proton rest mass
$p_\mu = (E, \vec{p}_\mu)$	Four-momentum of the incident lepton
$p'_\mu = (E', \vec{p}'_\mu)$	Four-momentum of the scattered lepton
$P = (M, \vec{0})$	Four-momentum of the target nucleon
$q = p_\mu - p'_\mu = (v, \vec{q})$	Four-momentum transfer
$Q^2 = -q^2 \cong 4EE' \sin^2(\theta_\mu/2)$	Invariant mass squared of virtual photon
$v = P \cdot q/M = E - E'$	Energy of the virtual photon
$\theta_\mu$	Muon scattering angle
$x = Q^2/2Mv$	Bjorken scaling variables
$y = v/E$	Inelasticity parameter

Table 2: Kinematic cuts applied to the data sample. $p'_\mu$ , $\theta_\mu$ are momentum and angle of the scattered muon $p_{had}$ is the momentum of the hadron in the laboratory system				
Beam energy (E)	[GeV]	100/120	200	280
$Q^2$ min	[GeV <sup>2</sup> /c <sup>2</sup> ]	2	2	5
$v$ min	[GeV]	10	30	50
min. x		0.02	0.02	0.02
$\theta_\mu$ min	[mrad]	16.0	14	14
$p'_\mu$ min	[GeV/c]	20	30	40
$y (=v/E_{beam})$ max		0.85	0.85	0.85
$p_{had}$ min	[GeV/c]	3	3	5

Table 3: Event statistics after the event selection, obtained from the data taken in 1984/85 with different heavy target setup

Beam Energy E	Number of events after event selection (see table. 2)			
	D <sub>2</sub>	C	Cu	Sn
<u>Tgt. set up I</u>				
100/120 GeV	35670	8800	26790	6660
200 GeV	16800	6930	13075	4560
280 GeV	5360	-	3650	-
<u>Tgt. set up II</u>				
100 GeV	192130	-	138890	-
280 GeV	69440	-	45220	-

Table 4: List of sources for systematic uncertainties, together with the estimate of the systematic error of hadron multiplicity ratios

Source of systematic uncertainty	Estimate of systematic error
Electron contamination	2 - 4% for $z > 0.5$ and $v > 150$ GeV 0.5 - 1% elsewhere
Radiative corrections	1 - 1.5% for $x < 0.06$ and $y > 0.65$ < 0.2 - 0.5% elsewhere
Systematic error in measurement of muon and hadron momentum	< 0.4%
Track selection	< 0.5%
Software reconstruction efficiency	< 0.2 - 0.4%
Secondary interactions in the target	< 0.5%

Table 5: Ratio of partial integrals  $R_A$  of differential energy distributions of charged hadrons integrated over  $Q^2$ ,  $v$  and  $x$  within the cuts given in table 1

	$\langle v \rangle$ [GeV]	$\langle x \rangle$	$\langle Q^2 \rangle$ [GeV <sup>2</sup> /c <sup>2</sup> ]	$R_A$	error stat. syst.
C/D <sub>2</sub>	52	0.14	10.2	1.018 ± 0.034 ± 0.005	
Cu/D <sub>2</sub> (Tgt set up I)	62	0.13	12.3	0.952 ± 0.015 ± 0.010	
Cu/D <sub>2</sub> (Tgt set up II)	62	0.14	10.6	0.946 ± 0.008 ± 0.005	
Sn/D <sub>2</sub>	62	0.13	11.8	0.917 ± 0.026 ± 0.01	

## Figure Captions

- Fig. 1 a) The EMC forward spectrometer used to measure the spin asymmetries on a polarised target and hadron distributions on nuclear targets (fig. b). For the last experimental runs the polarised target was replaced by an extended D<sub>2</sub> - Cu target (fig. c).
- Fig. 2 Definition of the muon and hadron variables used in this analysis.
- Fig. 3 Differential hadron multiplicity:  $1 / N_{\mu} \cdot dN^h / dz_h$  as a function of  $z_h$  for Cu and D<sub>2</sub>. The statistical errors are of a similar size to the symbols; the systematic errors are not shown.
- Fig. 4 Ratio of  $z$  distributions of nuclear targets relative to D<sub>2</sub>. The results on Cu/D<sub>2</sub> shown in fig. 4b are obtained from the high statistics run with the extended target. The errors for multiplicity ratios shown in the following figures always include the error due to the uncertainty in the correction for electron contamination (see text).
- Fig. 5 Ratio of the partial integrals  $\int_{0.2}^1 dz_h 1 / N_{\mu} dN / dz_h$  as a function of  $v$  for Cu/D<sub>2</sub>.
- Fig. 6a)  $v$ -dependence of ratios of the partial integrals in two  $Q^2$  bins.  
 b)  $v$ -dependence of ratios of the partial integrals in two  $x$  bins.
- Fig. 7 Ratio of the differential hadron multiplicity distribution:  $1 / N_{\mu} dN^h / dp_{\perp}^2$  as a function of  $p_{\perp}^2$  for Cu and D<sub>2</sub> in two  $v$  intervals.
- Fig. 8 Ratio of  $\langle p_{\perp}^2 \rangle$  of hadrons with  $z_h > 0.2$  as a function of  $v$  for Cu/D<sub>2</sub>.
- Fig. 9 Hadron multiplicity distribution as a function of the azimuthal angle  $\varphi$ , for Cu and D<sub>2</sub> in the highest  $v$  and  $z_h$  bin studied here; the distribution is normalised to the number of hadrons in that bin. Dashed and full line represent fits to the data (see text).
- Fig. 10  $\langle \cos(\varphi) \rangle$  as a function of  $W^2$  and  $z_h$ , separate for Cu and D<sub>2</sub>.
- Fig. 11 Ratio of  $\varphi$  distribution  $r(\varphi)$  Cu/D<sub>2</sub> for the same bin in  $W^2$  and  $z$  as in fig. 9; the full line is a fit to the data.

Fig. 12a) Dependence of nuclear absorption in the fast hadron production ( $z_h > 0.2$  compared with predictions of models for intranuclear reinteraction: the smooth curves are:

1) 1-scale model:  $\tau_h \sim E_{had}$ ;  $\sigma_q = 0$  mb

2-4) 2-scale model: 2)  $\sigma_s = 0$ mb; 3)  $\sigma_s = 20$ mb, in both cases  $\sigma^* = 0$ mb

4)  $\sigma_s = 20$ mb and  $\sigma^* = 0.75$ mb

Systematic and statistical errors of the results of [13] are shown separately.

b) Sketch to elucidate the model involving two space-time scales  $\tau_c, \tau_h$ .

Fig. 13 Comparison of the measured ratio of  $z$  distributions from Cu and  $D_2$  in the low  $v$  interval with predictions of nuclear dependent fragmentation functions for the ratio of  $z$  distributions Cu/ $D_2$ . Full line: harder fragmentation function in Cu [48] (see text) dashed/dotted line: rescaling of  $D_q^h(z_h, \xi Q^2)$  with different rescaling parameter  $\xi$  [45,46].

Fig. 14 Relationship between  $\langle k_{\perp} \rangle$  and  $\langle \cos(\varphi) \rangle$  for high  $v$  and  $z_h > 0.4$ ; the straight line is a fit to the results of the Monte Carlo calculation of [53,54].

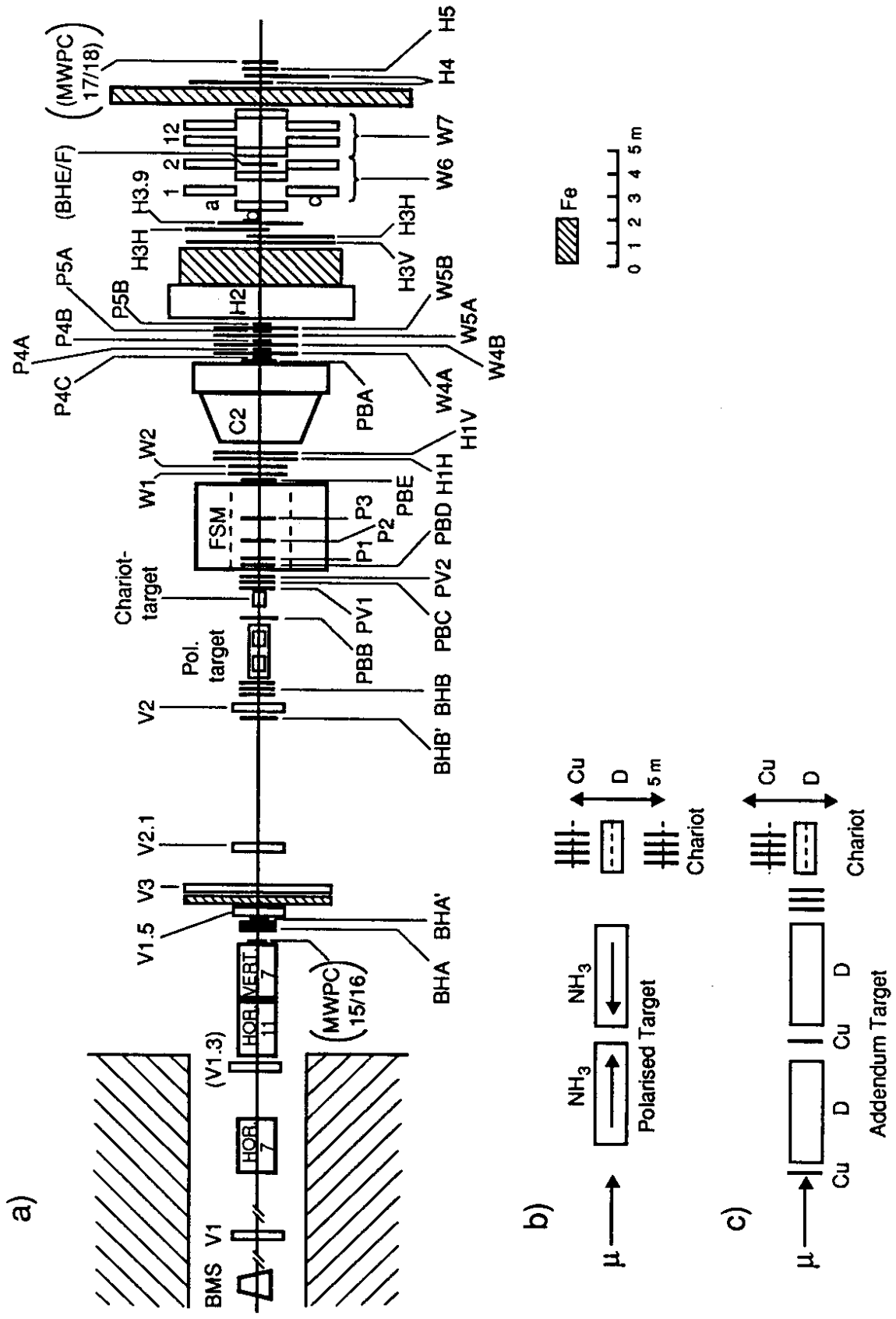


FIG. 1

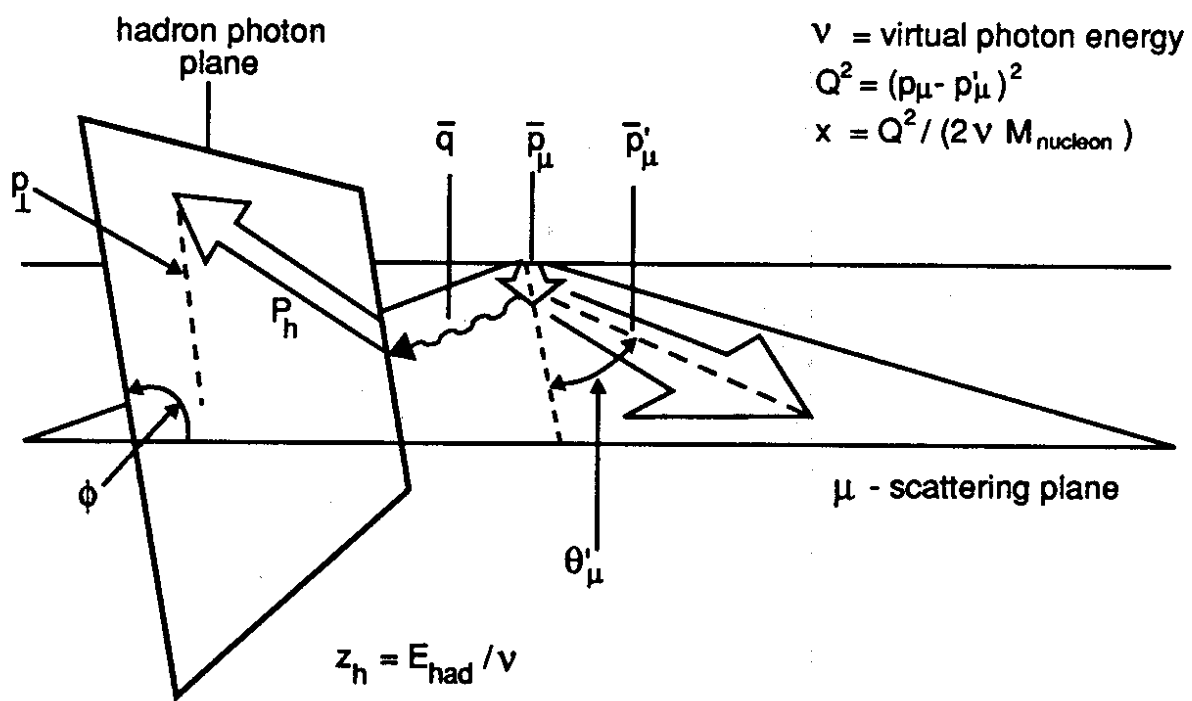


FIG. 2

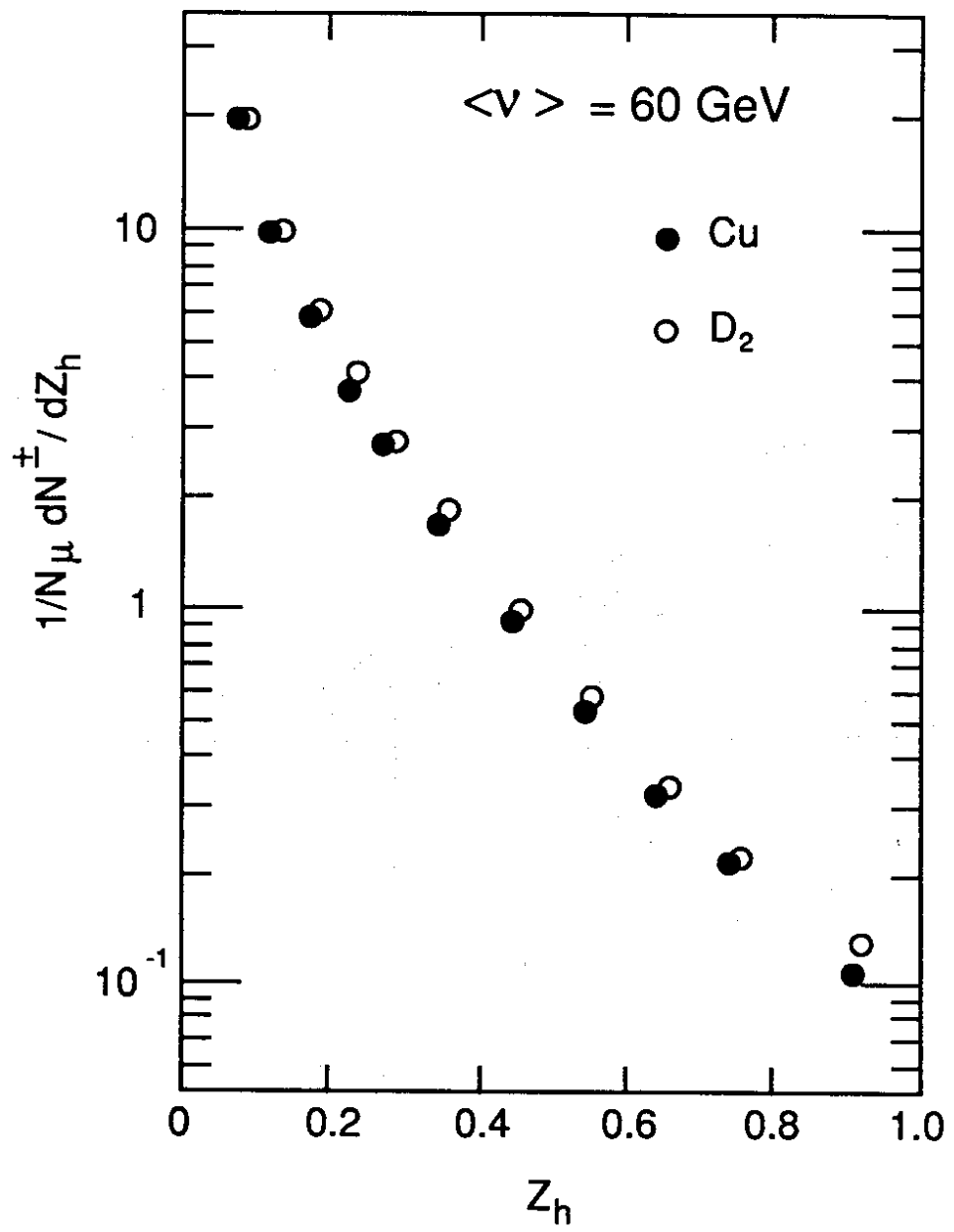


FIG. 3



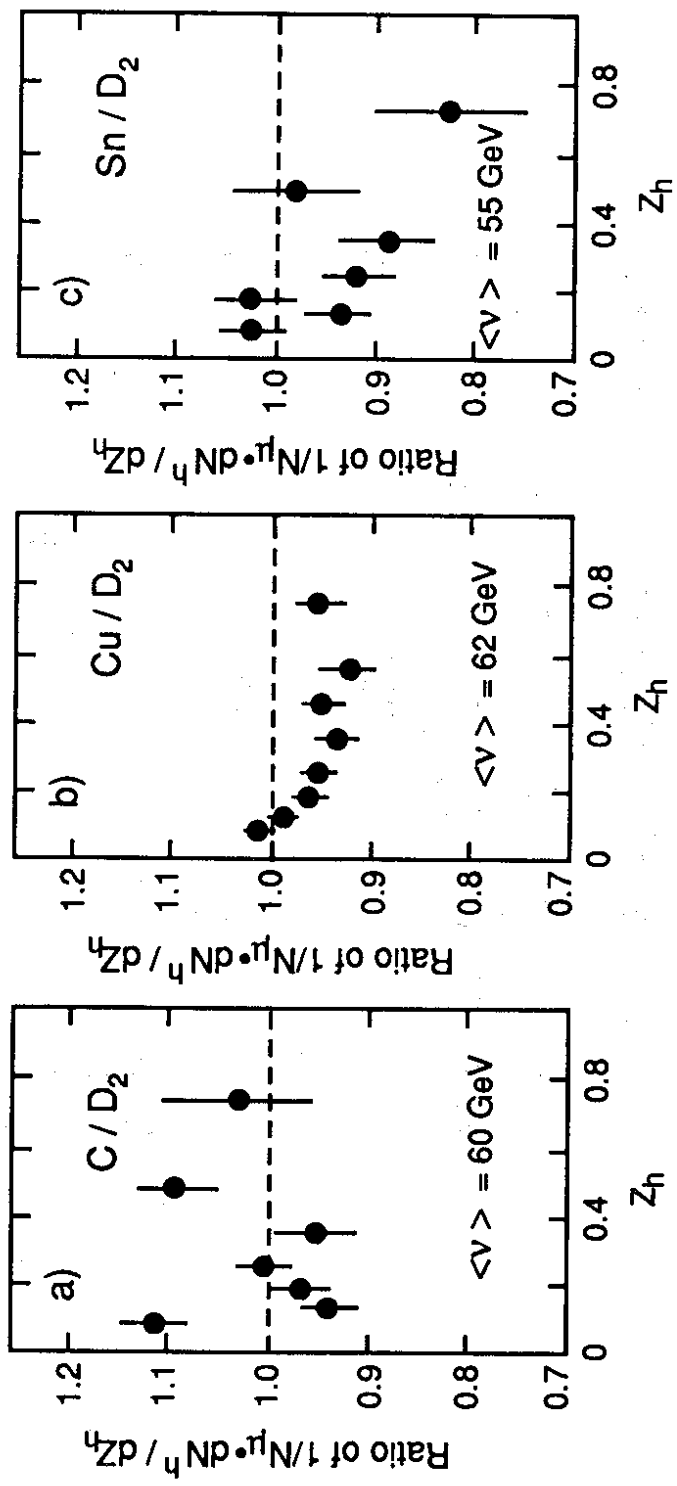


FIG. 4

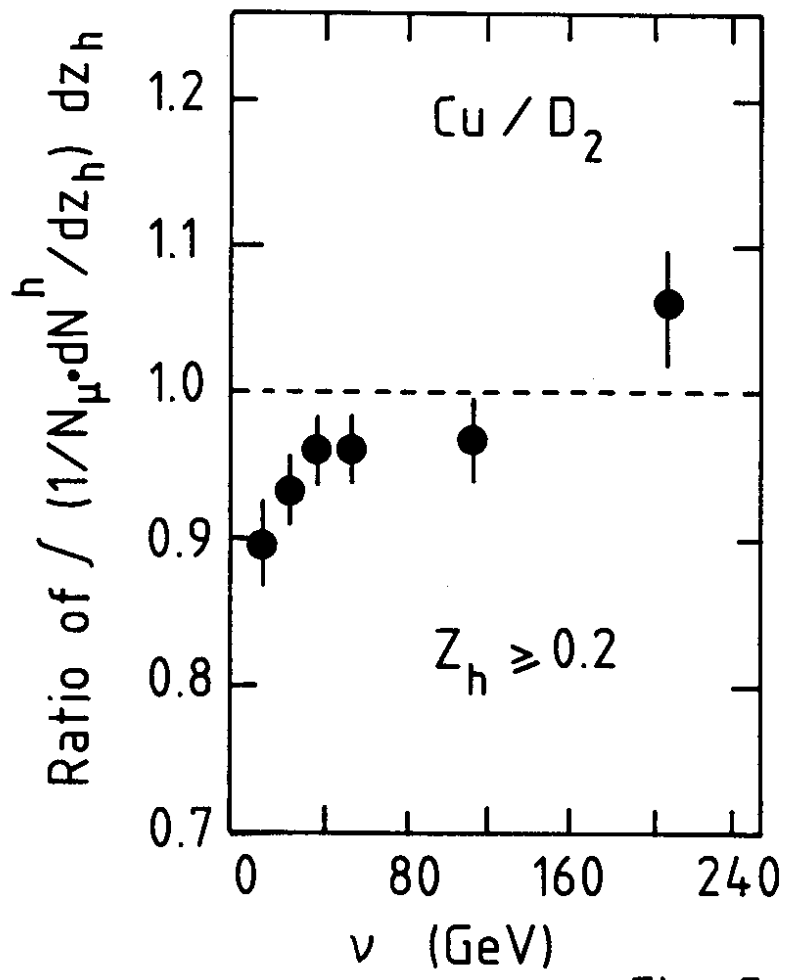


Fig. 5

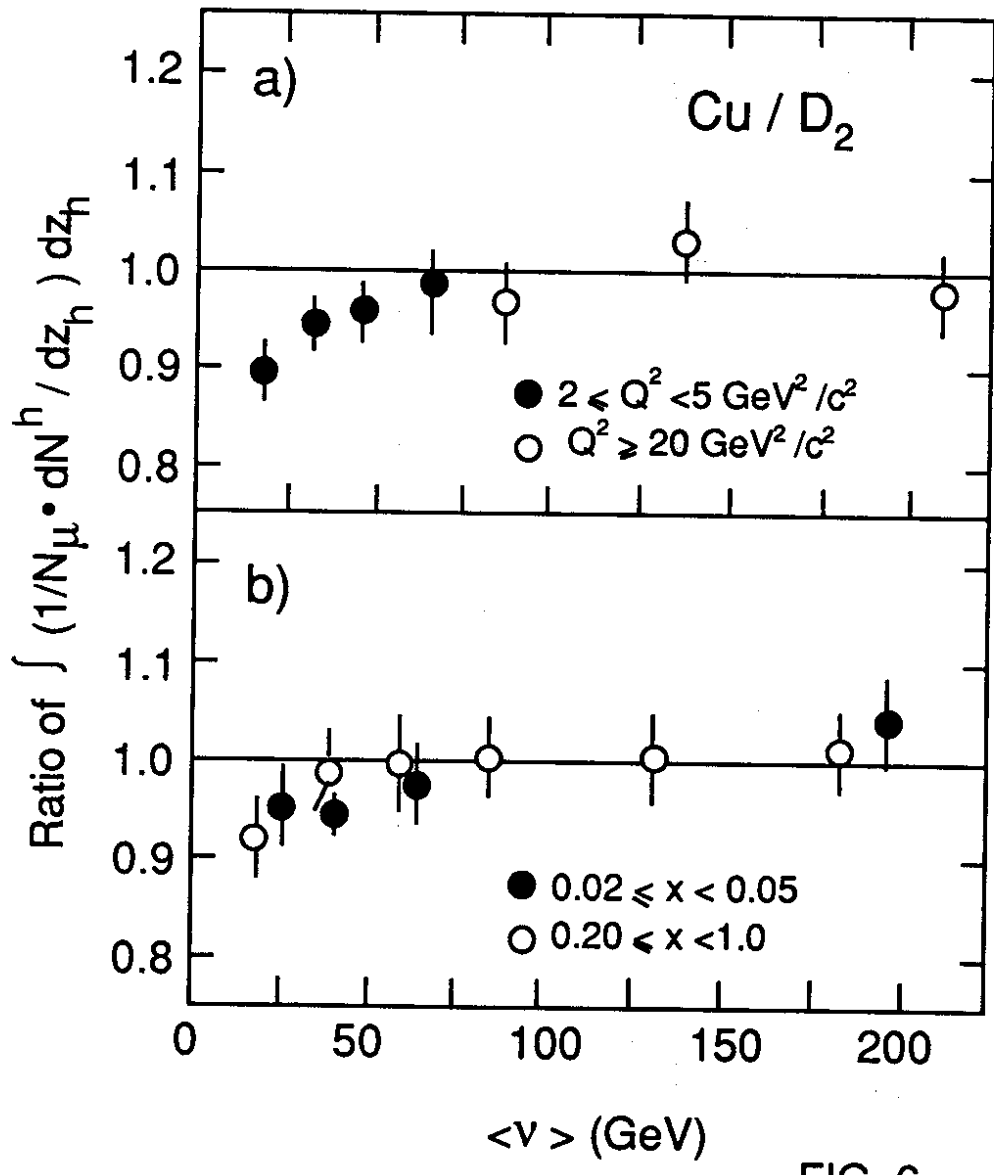


FIG. 6

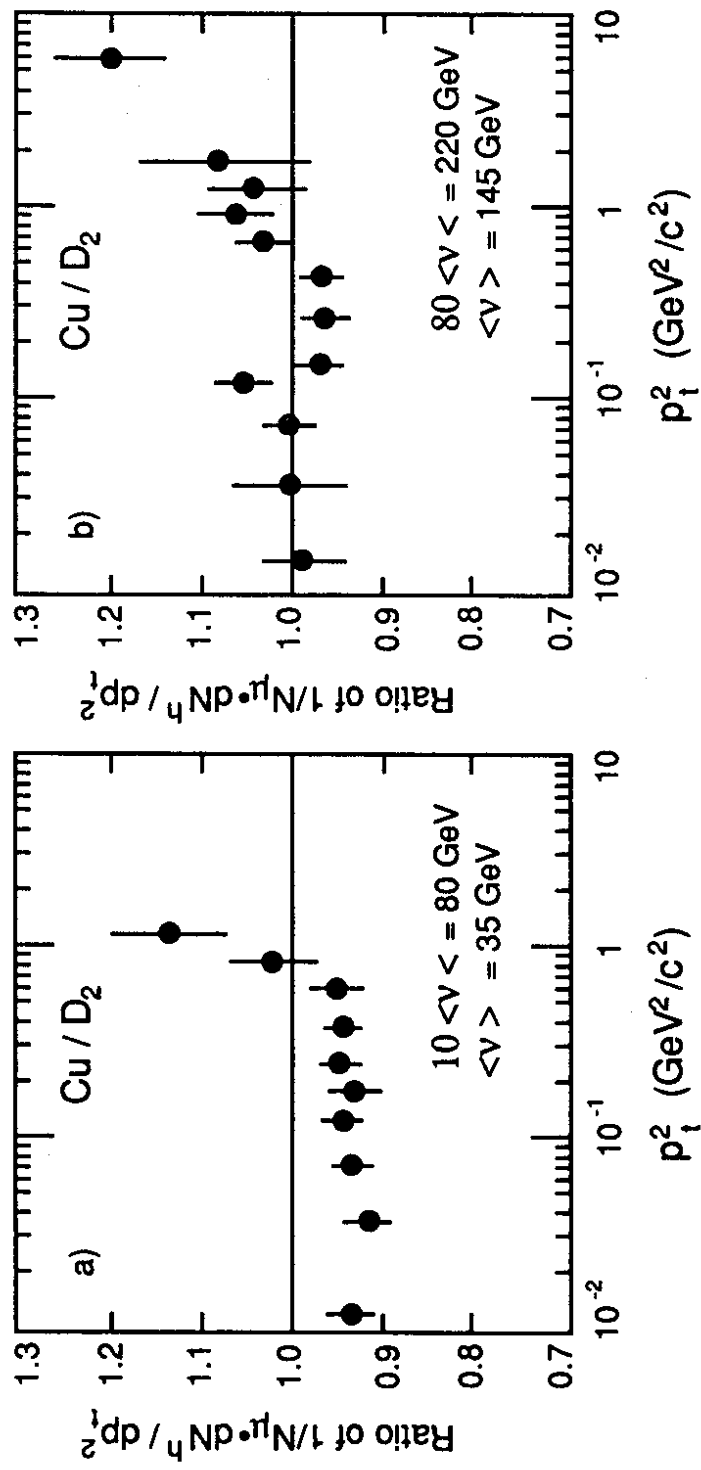


FIG. 7

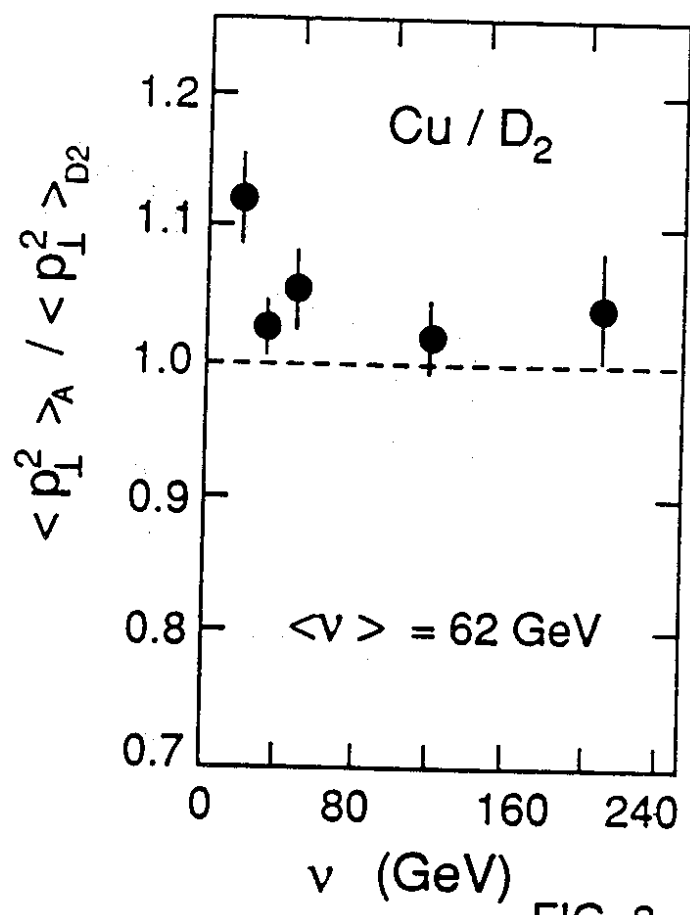


FIG. 8

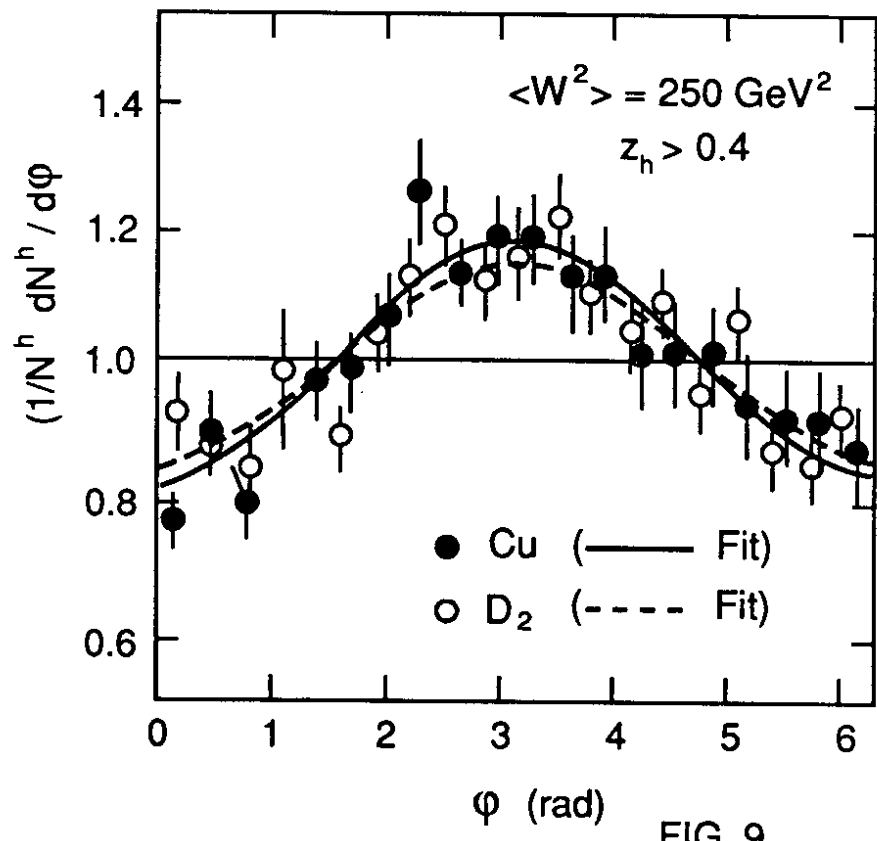


FIG. 9

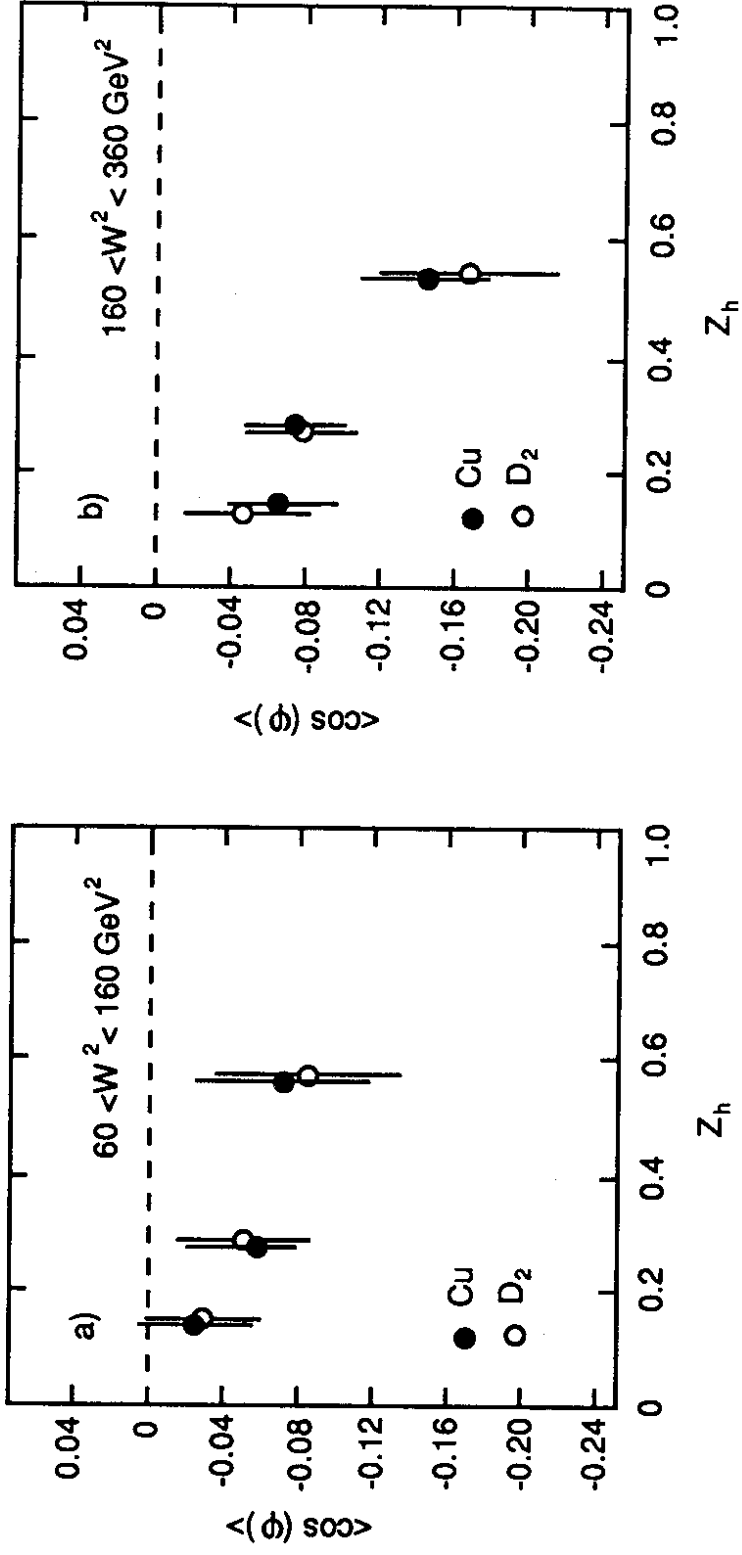


FIG. 10

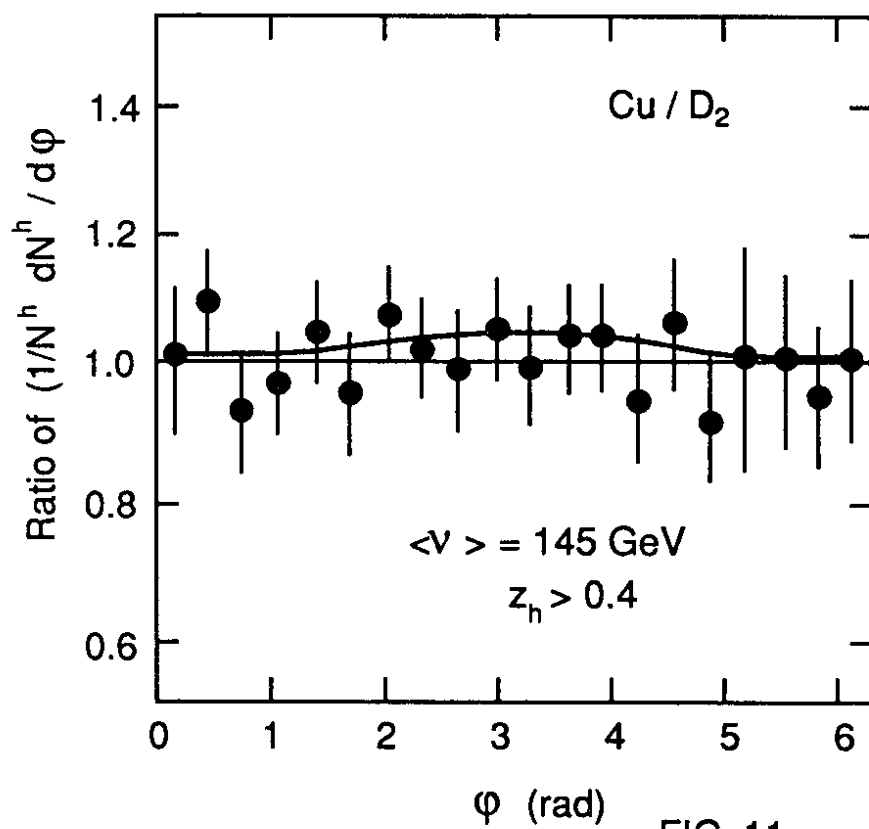


FIG. 11



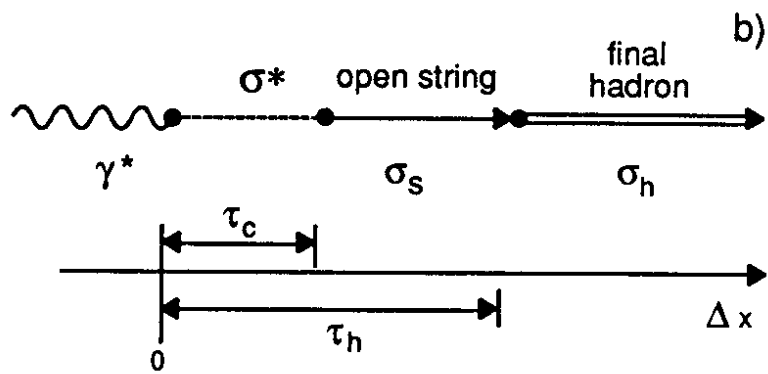
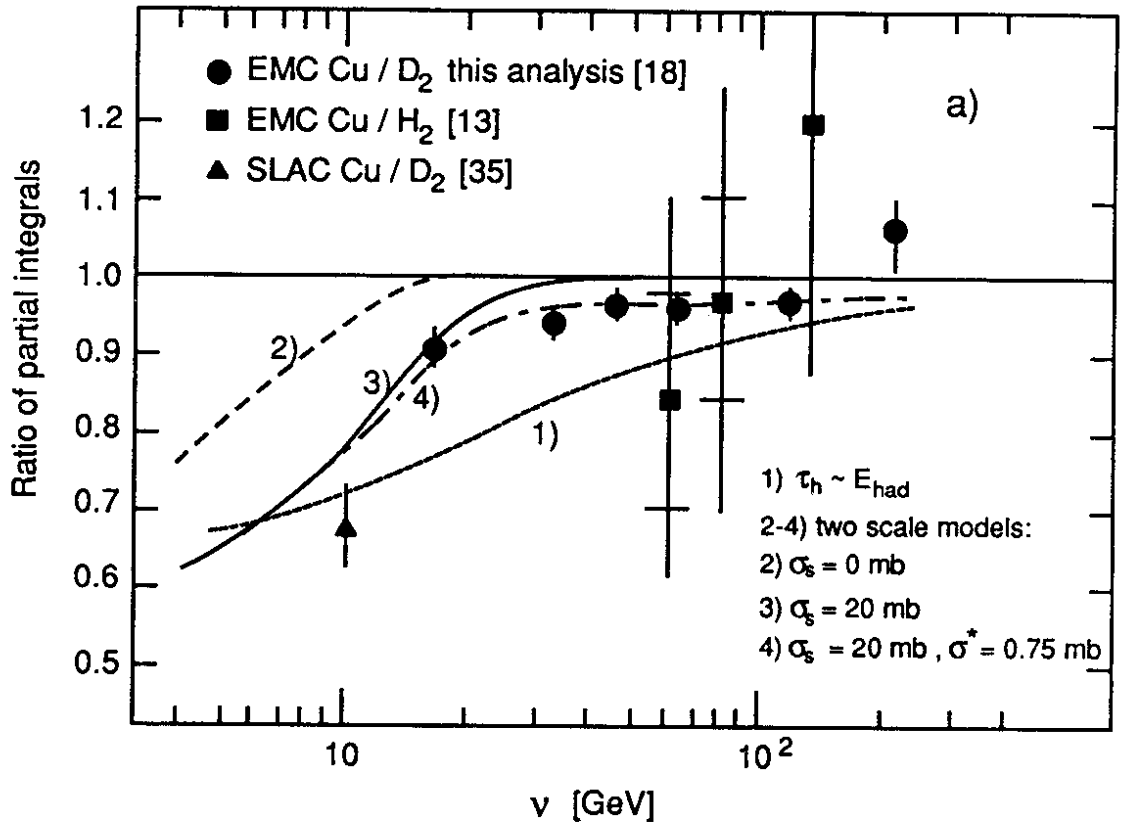


FIG. 12

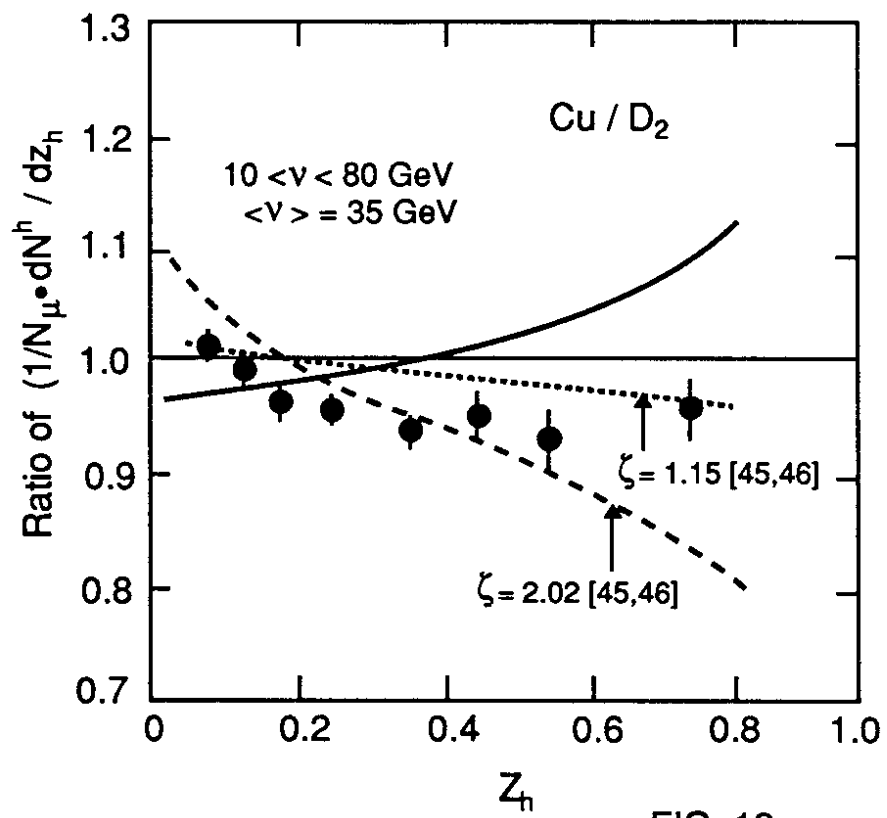


FIG. 13

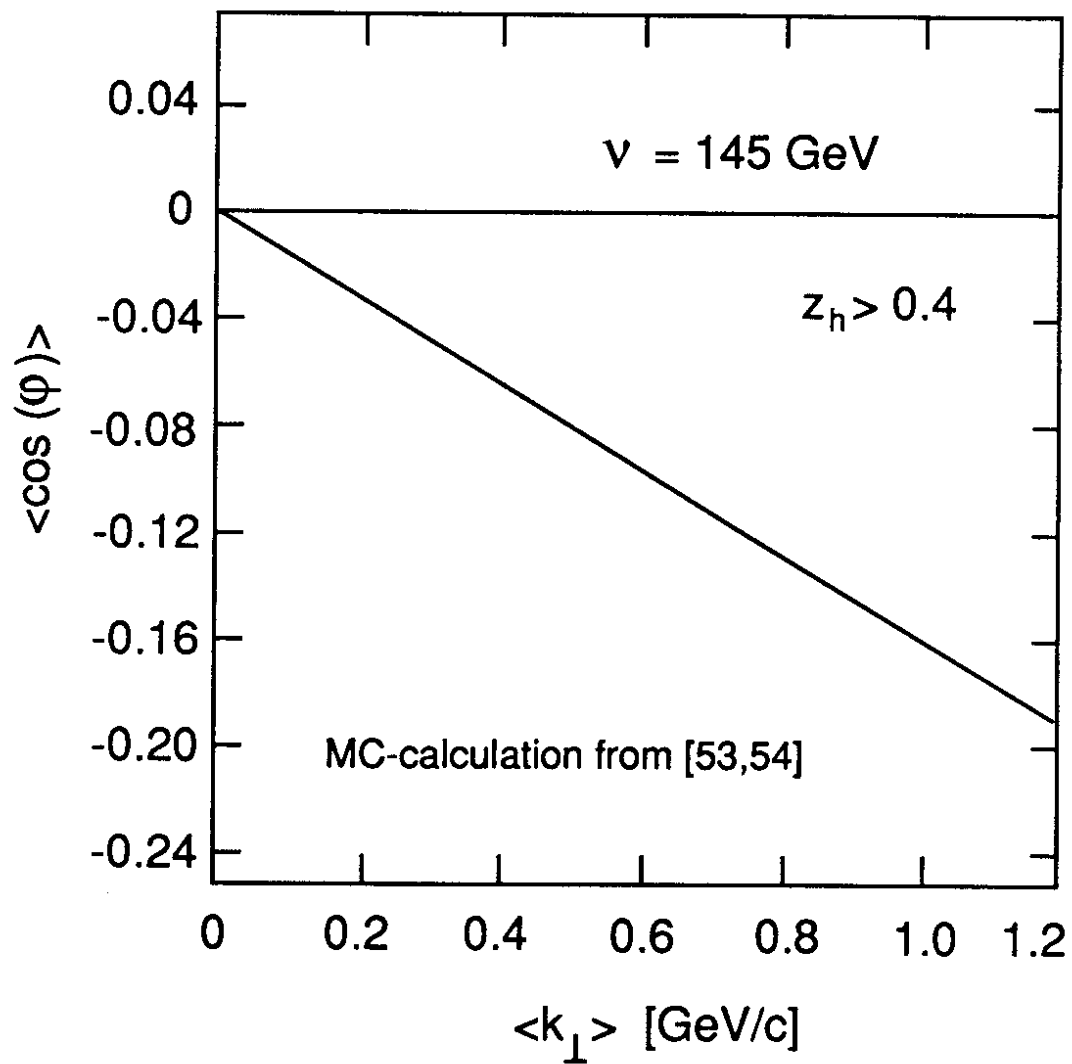


FIG. 14